DTU Library

The dynamic behavior and intrinsic mechanism of CO$_2$ absorption by amino acid ionic liquids

Tong, Jiahuan; Zhao, Yuanyue; Huo, Feng; Guo, Yandong; Liang, Xiaodong; von Solms, Nicolas; He, Hongyan

The dynamics behavior and intrinsic mechanism of CO_2 absorption by amino acid ionic liquids

Jiahuan Tong[a,b], Yuanyue Zhao[a,c †], Feng Huo[a*], Yandong Guo[c], Xiaodong Liang[b], Nicolas von Solms[b], Hongyan He[a]

[a] *Beijing Key Laboratory of Ionic Liquids Clean Process, Institute of Process Engineering, Chinese Academy of Sciences, Beijing 100190, P.R. China*

[b] *Department of Chemical & Biochemical Engineering, Technical University of Denmark, DK 2800 Kgs. Lyngby, Denmark*

[c] *College of Mathematics Science, Bohai University, Jinzhou 121013, PR China*

ABSTRACT:

Reducing carbon dioxide emissions is one of the possible solutions to prevent global climate change, which is urgently needed for the sustainable development of our society. In this work, easily available, biodegradable amino acid ionic liquids (AAILs) with great potential for CO_2 absorption in the manned closed space such as spacecraft, submarines and other manned devices are used as the basic material. Molecular dynamics simulation and ab initio calculation methods were performed for 12 AAILs ([P4444][X] and [P66614][X], [X]= X=[GLy]$^-$, [Im]$^-$, [Pro]$^-$, [Suc]$^-$, [Lys]$^-$, [Asp]$^{2-}$), the dynamic characteristics and the internal mechanism of AAILs to improve CO_2 absorption capacity were clarified. Based on the analysis of structural and the interaction energy including van der Waals and electrostatic interaction, revealed the fact that the anion of ionic liquids dominates the interaction between CO_2 and AAILs. At the same time, the CO_2 absorption capacity of AAILs increases in the order: [Asp]$^{2-}$ < [Suc]$^-$ < [Lys]$^-$ < [Pro]$^-$ < [Im]$^-$ < [Gly]$^-$. Meanwhile, the synergistic absorption of CO_2 by multiple-site of amino and carboxyl groups in anion was proved by DFT calculation. These findings show that the anion of AAILs can be an effective factor to regulate the CO_2 absorption process, which can also provide guidance for the rational and targeted molecular design of AAILs for CO_2 capture, especially in the manned closed space.

KEYWORDS: Ionic liquids, CO_2 absorption, Molecular dynamics simulation, manned closed system.

—————————————————————

† J. Tong and Y. Zhao contribute equally to this work.

1. Introduction

With the burning of fossil fuels, excessive emissions of CO_2 caused by automobile emissions and human activities, global warming and ecosystem changes have become one of the most serious challenges of environmental problems.[1-3] As a rich, non-toxic, and easily available renewable carbon resource, CO_2 has a wide range of applications in the fields of the chemical industry, oil and gas exploration, agriculture, tobacco, and firefighting. Separation and absorption of CO_2 have become a hot topic of common concern in academia, industry, and the international community.[4,5] At present, traditional CO_2 absorption methods include adsorption and membrane separation, *etc.*, all of which are realized by using effective absorption materials and solvents.[6,7] Therefore, the absorption performance of CO_2 is closely related to the development and selection of absorption materials and solvents.

As a new type of green solvent and medium, ionic liquids (ILs) is an alternative to traditional organic solvent, because of its unique properties such as high thermal stability, low melting point, wide electrochemical window, and adjustable structures, *etc.*.[8,9] In recent years, a large number of experimental and theoretical studies have reported that ILs can be used as solvents to effectively absorb CO_2 through traditional absorption and adsorption methods.[10-12] Wang *et al.*[13] developed a novel integrated system consisting of the imidazolium-based ILs and organic superbase for the absorb of CO_2 under atmospheric pressure. The results have shown that the integrated system could quickly, effectively, and reversibly absorb about one mole of CO_2 per mole of ILs. In another study, an imidazole-ring functionalized copolymer for CO_2 separation were synthesized by Lee *et al.*[14] They investigated the solubility and permeability of CO_2. Their findings showed that the excellent CO_2 separation performance was achieved by this material, with a CO_2 permeability of 148.6 Barrer and CO_2/N_2 and CO_2/CH4 selectivity of 65.3 and 35.0, respectively. These conventional ILs and ILs-based materials have been proven to have many outstanding effects in CO_2 absorb; however, most of the researches are based on open spaces currently. Due to the harsh experimental conditions in enclosed spaces, there are few studies on the absorb of CO_2 in manned closed systems such as spacecraft and submarines. Therefore, the development of new solvents and materials with low energy consumption, high cycle stability and no by-products is a key challenge in the field of gas absorption in confined spaces.

Amino acids are environmentally friendly and biodegradable agents and contain no halide ions. Amino acid ionic liquids (AAILs), a novel type of ILs with a primary amine (–NH_2) functional group which are synthesized using natural amino acids as raw materials.[15,16] Similar to conventional ILs, AAILs also has the characteristics of conventional ILs.[17] Meanwhile, AAILs have many unique properties such as low toxic, strong biocompatibility, biodegradable and hydrogen bond network structure, which can dissolve many living substances, such as DNA, cellulose, carbonyl compounds, *etc.*. Ohoo *et al*. synthesized AAILs from

1   20 kinds of natural amino acids for the first time in 2005.[18] By analyzing the acidity, hydrogen bonding

2   ability and steric factors of amino acids, they showed the importance of amino acid side groups on the

3   properties of AAILs. After that, many studies have reported that compared with conventional ILs, AAILs

4   can absorb CO_2 more effectively.[19,20] Moghadam $et\ al.$[21] separated the low concentration of CO_2 from the

5   mixtures of CO_2/N_2 using the AAIL-based membrane. Their work indicated AAIL-based membrane

6   showed high CO_2 permeability, is around 52000 bar, and high CO_2/N_2 selectivity, is around 8100.

7   Seyedhosseini $et\ al.$[22] conducted computational studies on the absorption of CO_2 by N7, N9-

8   dimethyladeninium cation with amino acid anions ([dMA][X] X= Gly, Ala, Val, Leu, and Ileu). They found

9   that an increase in the length of amino acid side chains increases the ability to absorb of CO_2. Recently,

10 Kang $et\ al.$ analyzed the CO_2 absorption mechanism of dual amino group functionalized imidazolium

11 AAILs by ^{13}C NMR and FT-IR spectroscopy. Their work indicated that the number of amino groups in the

12 ILs affects their CO_2 absorption capacity.[23] Meanwhile, Shaikh $et\ al.$[15] Using density functional theory

13 (DFT) and molecular dynamics methods to study the reaction mechanism of tetramethylphosphonium

14 glycinate ([P_{1111}][Gly]) and tetrabutylphosphonium glycinate ([P_{4444}][Gly]) AAIL to absorb CO_2, and the

15 effect of AAILs on CO_2 adsorption in the presence of pure AAIL form and explicit water was explored.

16 The results show that in the presence of water, the interaction between cations and anions decreases, thereby

17 reducing the diffusion coefficient of cations, while in the presence of 10% water, the viscosity of the

18 compound increases, thereby reducing carbon dioxide absorption. At the same time, it was found that the

19 lower free volume and higher density produced in [P_{1111}] [Gly] will inhibit the absorption of CO_2. At the

20 same time, different from the traditional closed space absorb CO_2 methods (including non-renewable [24],

21 physicochemical regeneration, and solid material-based adsorption methods[25]), AAILs are bio-renewable

22 and have potential advantages and application feasibility in the field of CO_2 absorb in manned closed system.

23   To design and choose appropriate ILs for carbon absorb, it is important to understand their properties

24 and molecular interactions involved in the corresponding processes. Fundamental molecular insights are

25 useful for understanding the thermodynamic, structural, physicochemical, and dynamic behaviors of AAILs.

26 However, so far, there are few systematic theoretical studies on CO_2 absorb using AAILs. Moreover, most

27 studies lack detailed discussions on "how the cations and anions of AAIL affect the physical and chemical

28 properties of the gas liquid system" and "what role does AAILs play in capturing CO_2 molecules". To do

29 this, we conducted MD simulations and the DFT to examine the effect of 12 types of

30 tetrabutylphosphonium-based and trihexyltetradecylphosphonium-based AAILs ($viz.$ [P4444][X] and

31 [P66614][X], X=[Gly], [Im], [Pro], [Suc], [Lys], [Asp]) on CO_2 absorb. The physicochemical and

32 dynamics properties of these AAILs-CO_2 systems, such as density, self-diffusion coefficient and residence

33 time were calculated. Further the microstructures of AAILs were analyzed in various AAILs-CO_2 by

evaluating the radial distribution function ($g(r)$), spatial distribution function (SDF), and ionic coordination number (N). Meanwhile, van der Waals and coulombic energy between CO_2 and AAILs and the stable absorption site were explored by DFT analysis. Our current study will help to understand the reaction mechanism that will serve as a guide to design new ionic liquids with improved CO_2 absorb capability in manned closed system.

2. Simulation Details

2.1 Molecular Dynamics Simulations

All the MD simulations in this work were conducted for 512 CO_2 molecules in a periodic boundary box containing 512 pair of tetrabutylphosphonium-based and trihexyltetradecylphosphonium-based AAILs (*viz.* [P_{4444}][X] and [P_{66614}][X], X=[Gly], [Im], [Pro], [Suc], [Lys], [Asp]) at 300K, 350K and 400K (Figure 1). The all-atom optimized potential for liquid simulations force field (OPLS-AA) was used to describe the atom types for all-atom types in our MD simulations. The partial charges of CO_2 and AAILs were obtained by the restrained electrostatic potential (RESP) procedure. [26,27] The initial configurations of the MD simulations were constructed by using the Packmol package.[28] All the MD simulations were carried out in the Lammps software.[29] The Verlet algorithm is employed to integrate Newton's equations of motion which the time step is 1.0 fs. Meanwhile, the van der Waals interaction and the electrostatic interaction are treated with the Lennard-Jones potential and the Particle Mesh Ewald (PME) technique, respectively. For each simulation system is relaxed in the canonical ensemble (NVT) and the isothermal-isobaric ensemble (NPT) for the first 4ns. The production simulation in the NPT ensemble is carried out for 20ns and in the NVT ensemble to achieve the configurational equilibria for 30 ns. The trajectories are recorded at every 0.1ps for further analysis during the simulation.

2.2 Ab Initio Calculations

The structures for all the cations and anions of AAILs, and CO_2 were optimized at the B3LYP/6-311++G** level by Gaussian 09 software.[30] For anion-CO_2, the typical configuration in the MD trajectory is randomly selected as the initial structure. After optimization, 15 types of lower energy anion-CO_2 structures were selected on the B3LYP/6-311++G** level through Gaussian 09 software for further optimization. Then, the structure with the lowest energy and no imaginary frequency was obtained.
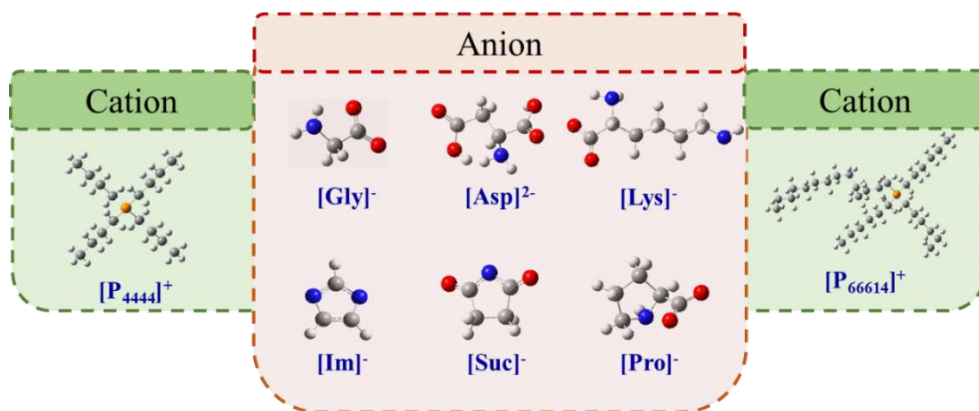
Figure 1. Structures of the AAILs involved in our MD simulations.

3. Results and Discussions

3.1 Liquid Density

In this work, the CO_2-AAILs density can be obtained in the equilibrium simulation of the 20ns NVT ensemble. The density of all AAILs and CO_2-AAILs at 300K was calculated and listed in (Table 1) in which the experimentally measured densities of the pure AAILs are also reported. Clearly, it is found that for a common anion, $[P_{4444}]^+$-type AAILs has a higher density than the $[P_{66614}]^+$-type AAILs, except for $[Asp]^{2-}$ system, while for a common cation ($[P_{4444}]^+$ or $[P_{66614}]^+$), $[Im]^-$-type AAILs have the lowest density in all systems. The results show that the size of the cation/anion of AAILs can affect the density of CO_2-AAILs system, *viz.,* the density decreases with the increased size of cation, on the contract, an opposite effect was observed for the anion of AAILs. The same conclusion was also reported by Sedden *et al.*.[31] Meanwhile, regardless of the type of cation, the $[Asp]^-$-type system has the highest density for the amino acid anion type. It reflects a fact that the carboxyl groups(-COOH) and the number of carboxyl groups have an important influence on the density of the CO_2-AAILs system. Due to the addition of carboxyl groups, the interaction between carboxyl groups and CO_2 will increase, which will lead to an increase in system density. (The interaction will be discussed in detail below). Meanwhile, the density of the chain-type amino acid anion corresponding to the CO_2-AAILs system is slightly greater than that of the cyclic-type anion, which the order of the density for $[P_{66614}]^+$-type AAILs is $[Asp]^->[Lys]^->[Gly]^->[Pro]^-$. Additionally, the simulated density of the pure AAILs for simulated values is higher than that of the experimental values, which is consistent with the typical deviation of the MD simulation allowed (*i.e.,* less than 3%). Since under the AA force field, the long chain of cations increases the influence of polarizability of AAILs, which tends to produce higher density. However, this work focuses on the absorption behavior of CO_2 in AAILs. In future

1 work, we will improve the force field and increase the accuracy of liquid density by carefully adjusting

2 certain parameters or increasing the influence of the polarization rate.

3

4 **Table 1.** Experimental and simulated density (unit: g/cm^3) of all CO_2-AAILs and pure AAILs systems.

Cation	Anion	$\rho_{sim-co2/AAILs}$	$\rho_{sim-AAILs}$	$\rho_{exp-AAILs}$[32,33]	Error (%)
	[Gly]$^-$	0.94	0.93	0.96	2.67
	[Pro]$^-$	0.96	0.96	0.99	2.78
	[Im]$^-$	0.92	0.91	--	--
[P$_{4444}$]$^+$	[Lys]$^-$	0.96	0.95	0.97	1.64
	[Asp]$^{2-}$	0.99	--	--	--
	[Suc]$^-$	1.02	--	--	--
	[Gly]$^-$	0.91	0.89	0.90	0.81
	[Pro]$^-$	0.90	0.89	0.89	0.08
	[Im]$^-$	0.88	0.88	0.88	0.82
[P$_{66614}$]$^+$	[Lys]$^-$	0.93	--	--	--
	[Asp]$^{2-}$	1.04	--	--	--
	[Suc]$^-$	0.92	--	--	--

5

6 3.2 Dynamics behaviors

7 3.2.1 Diffusion Property

8 A high self-diffusion rate can improve the rate of absorption of CO_2 by AAILs. Therefore, the self-

9 diffusion coefficient (D) of the anion/cation of AAILs and CO_2 in the CO_2-AAILs system was calculated

10 according to Einstein's equation, which is a function of the ion mean square displacement (MSD) in the

11 system, as given in equation (1):

12

$$13 \quad D = \frac{1}{6} \lim_{t \to \infty} \frac{d}{dt} \langle \sum_{i=1}^{N} [\vec{r_i}(t) - \vec{r_i}(0)]^2 \rangle \tag{1}$$

14 where $\vec{r_i}(t)$ indicates the positional vector of the center of mass of the ith ion at a given time t. Meanwhile,

15 to distinguish the different time scales, the exponent β can be computed over a range of time scales using

$$\beta = \frac{d\log(\Delta r^2(t))}{d\log(t)} \tag{2}$$

To our best knowledge, at short times the motions of the ions are almost ballistic movement, so that $\beta > 1$. At long times after the molecules have undergone many collisions the systems should become normal linear diffusive behavior, and $\beta = 1$. In the intermediate-time range, the motion shows subdiffusive dynamics similar to a supercooled liquid, which is related to cage escape, and $\beta < 1$. [34] Therefore, in this work, the effect of CO_2 absorption on AAIL cation and anion dynamics was examined by mean MSD for all systems over the time interval (t) from the last 10 ns on NVT ensemble of MD trajectory, then the slope of the MSD-t plots for the time corresponding to $\beta \approx 1$ were linearly fitted (dotted line in Figure 2(a)). The self-diffusion coefficients of cation, anion for all AAILs and CO_2 have been obtained and shown in Table 2.
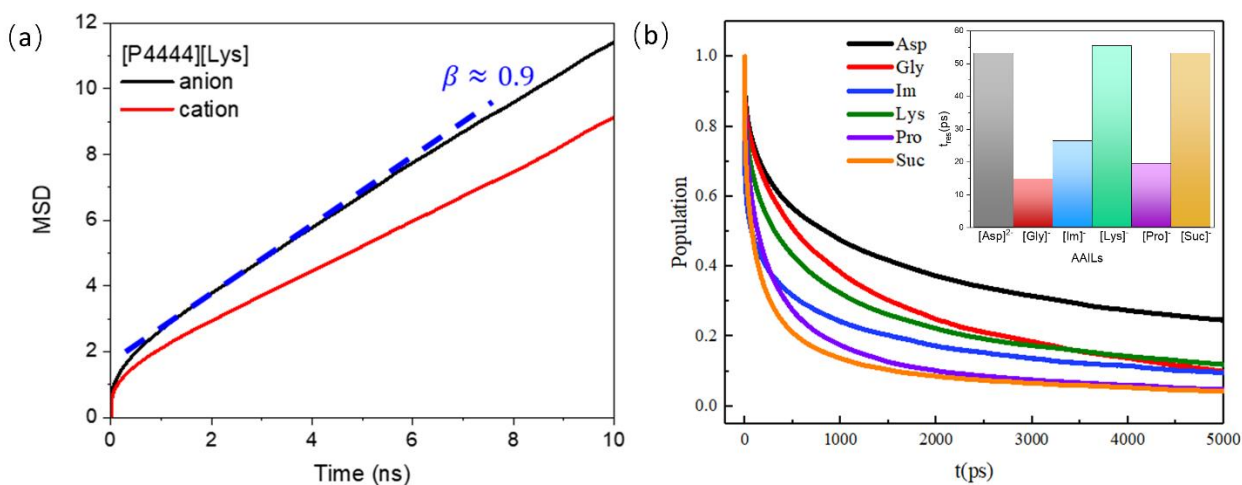
Figure 2. (a) The plots of mean square displacement (MSD) of $[P_{4444}]^+$, $[Asp]^{2-}$ *vs.* simulation time (t) in the $[P_{4444}]$ $[Lys]$-CO_2 system. (b) The residence time for CO_2-anion in all systems.

Comparing the CO_2-AAILs systems with different cations in Table 2, it is obvious that for the same type of anion, the self-diffusion coefficient of CO_2 in the $[P66614]^+$-type AAIL system is much higher than that of the $[P_{4444}]^+$-type (except for $[P_{66614}][Suc]$), as evidenced by the self-diffusion coefficient in Table 2. This phenomenon is opposite of density, where CO_2 diffuses faster in a large size of cation systems. The same conclusion has also been proved in different ILs. For example, Ren *et al.* investigated the different alkyl chain lengths of imidazole cations with the anion ($[TF_2N]^-$). It is found that the diffusion and solubility of CO_2 increase with the increased of cation length.[35] At the same time, due to the anion has a stronger coordination with the surrounding CO_2 molecular, the anion exhibits faster mobility than the cation in the

1 [P$_{66614}$][X] systems ([X]=[Gly], [Im], [Pro], [Suc], [Lys], [Asp]) (The coordination number of cation and

2 anion in AAILs will be discussed in detail later in the text). The same conclusions were drawn by Prakash

3 *et al.*[36] in their simulation study of the [P$_{4444}$] [Lys]-CO$_2$ system. Meanwhile, regardless of the AAIL cation

4 type, the self-diffusion coefficient of CO$_2$ has the largest value in [Asp]$^{2-}$-type AAIL, which is consistent

5 with the results found in the density. In addition, for the amino acid-type anion of both [P$_{4444}$] $^+$-type and

6 [P$_{66614}$] $^+$-type AAIL, the order of the self-diffusion coefficient of CO$_2$ follows: [Asp]$^{2-}$>[Gly]$^-$>[Pro]$^-$>[Lys]$^-$.

7 That is to say, for chain-type amino acid anions, the rate of CO$_2$ movement decreases as the increased of

8 length of the amino acid alkyl chain. At the same time, for the cyclic and chain amino acid anions with

9 similar size ([Asp]$^{2-}$ and [Pro]$^-$), the movement of CO$_2$ in the chain-type anions is greater than the cyclic-

10 type. We hypothesis that the diffusion of CO$_2$ in the AAIL system is related to the anion structure (the

11 interaction of CO$_2$ and the anion of the AAILs will be discussed in detail below). Besides, no matter what

12 the AAILs is, the self-diffusion coefficient of all ions increases as temperature increases (Table S1).

13

14 **Table 2.** Self-diffusion coefficients (unit: 10^{-12} m^2/s) of the cation/anion and CO$_2$ in all CO$_2$-AAILs systems.

D	[P4444]$^+$						[P66614]$^+$					
	[Gly]$^-$	[Pro]$^-$	[Lys]$^-$	[Asp]$^{2-}$	[Suc]$^-$	[Im]$^-$	[Gly]$^-$	[Pro]$^-$	[Lys]$^-$	[Asp]$^{2-}$	[Suc]$^-$	[Im]$^-$
Anion	1.47	0.84	1.68	2.44	1.58	0.65	1. 96	1.73	1.02	3.51	5.17	1.23
Cation	0.97	0.75	1.26	2.47	1.61	0.83	1.15	0.71	0.63	2.51	1.66	0.62
CO$_2$	56.21	51.43	39.66	72.73	53.67	51.29	94.35	66.41	61.18	101.36	45.46	93.53

15

16 **3.2.2 Residence Time**

17 Over time, the absorption and structure of CO$_2$ in AAILs fluctuates constantly. The residence time

18 between CO$_2$ and anion or cation was further calculated to consider the dynamical property of CO$_2$-AAILs.

19 Herein, the residence time correlation functions (R(t)) is calculated by

20
$$R(t) = \frac{1}{N_r} \sum_{n=1}^{N_r} \sum_{j} \langle \theta(r_i, 0)\theta(r_i, t) \rangle$$

Where $\theta(r,t)$ the heavyside step function, when the CO_2 molecule i stays in the first coordination shell, its value is 1; when it leaves the first solvation shell, its value is 0. N_r is the coordination number of the CO2 molecules in the first solvation shell and t is the time? The R(t) for the cation and anion in different AAILs are both shown in Figure 2(b). As expected, there is a strong positive correlation with the anion size, the residence time decreases in the order [Lys]⁻, [Asp]²⁻, [Suc]⁻, [Im]⁻, [Pro]⁻, [Gly]⁻ for anions around the CO_2. The shortest residence time for amine acid anion is [Gly]⁻, which should originate from its strong interaction energy. (We will discuss this in detail later). To the best of our knowledge, the fast diffusion of CO_2 is also meaningful for the capture of CO_2, which can promote the absorption and desorption process of CO_2 in ILs and reduce the related energy consumption. As shown in Table 2 and Figure 2(b), the residence time has a negative correlation with CO_2 diffusion (the order of the diffusion coefficient is opposite to the residence time for chain-type anion). At the same time, the chain length and the number of carboxyl groups also affect the absorption and diffusion of CO_2, that is, the shorter the chain and the larger number of -COOH group, the higher the absorption capacity. At the same time, in order to clarify the influence of temperature on the dynamic characteristics of CO_2 in AAILs, Figure S1 shows the change of CO_2 residence time at three different temperatures. Obviously, due to the high kinetic energy of CO_2, as the temperature increases, the residence time gradually decreases.

3.3 Mechanism of AAILs absorbing CO_2

3.3.1 Microstructural analysis of CO_2-AAILs

Exploring the structure between CO_2 molecules and AAIL at the micro-level is very important to understand the effect of CO_2 absorption. In general, the radial distribution function (RDF) and the spatial distribution function (SDF) from MD simulation are provide molecular insight into exploring the relative position of the cation/anion and CO_2 in the microstructure of CO_2-AAILs system. The center of mass of the RDF for anion-CO_2 and cation-CO_2 were shown in Figure 3(a) and (b) to investigate the effect of different types of AAILs on the distributions of the CO_2 molecular. Obviously, regardless of the AAILs and temperatures (Figure S2) the primary peak in the g(r) plots of the CO_2-anion is sharper and more intense; however, a weaker and broader peak exists between the cation and CO_2 molecules. At the same time, comparing Figure 3(a) and (b), the average position of the primary peak for CO_2-anion and CO_2-cation were calculated: 0.57 nm for the [P₄₄₄₄]⁺ cation and 0.46 nm for anions. This result indicated that due to the steric hindrance caused by the phosphorus atoms on the cations (both [P₄₄₄₄]⁺ and [P₆₆₆₁₄]⁺) with a large number of positive charges and with longer alkyl chains, the interaction between the CO_2 molecules and the cations is weak. At the same time, the anion of ILs dominates the interaction between CO_2 and AAILs, which is consistent with the investigations of the simulation study by Zhang *et al.*[12] and the experimental

1 study by Sergei *et al*..[37] To further reveal the influence of different anion structures on the effect of CO_2

2 absorption, the interaction between CO_2 and anion (Figure 3(b)) were carefully compared. Clearly, the

3 position of the primary peak of the CO_2-anion in the CO_2-[P_{4444}] [X] follow the order: [Lys]$^-$> [Asp]$^{2-}$>

4 [Suc]$^-$>[Pro]$^-$>[Im]$^-$> [Gly]$^-$. It reflects the fact that it is more effective to absorb CO_2 by chain-type AAILs,

5 rather than cyclic-type of AAILs. Meanwhile, by comparing the different chain lengths of the chain-type

6 structure of amino anion ([Gly]$^-$, [Asp]$^{2-}$, and [Lys]$^-$) for AAILs, we found that the distance between anions

7 and CO_2 decreases as the chain length increases. The results indicated that the alkyl chain in amino acid

8 anion will affect the interacting distance between anion and CO_2, *viz*., the alkyl chain hinder the free motions

9 of CO_2 moleclule in the CO_2-AAILs systems. It is the main reason why the diffusion rates of the CO_2 are

10 slow in the longer alkyl chain amino acid anions systems (Table 2). In addition, obviously, regardless of

11 the AAILs and temperatures (Figure S2), the primary peak in the g(r) plots of the CO_2-anion always appear

12 at the position of around 0.46-0.49 nm, indicating that the CO_2 always have strong coordination with the

13 AAILs and the structural stability is affected less by the temperature. To visually describe the spatial

14 distribution of CO_2 and AAILs, the spatial distribution function (SDF) for CO_2 molecule around different

15 types of anion for AAILs are further analyzed. As shown in Figure 3(c), for the cyclic-type anion (such as

16 [Suc]$^-$), the CO_2 molecule prefers to locate above and below the ring plane. However, the CO_2 exhibits a

17 strong affinity toward the most negatively charged oxygen atom on the -COOH group of the anions for

18 chain-type anion, which corresponds well with the RDF in Figure 4(b). Furthermore, since the coordination

19 number N(r), which represents the average number of CO_2 molecules within a sphere of radius *r* around the

20 mass of the center of anion/cation for AAILs. It could be used as a quantitative parameter to measure the

21 absorption capacity of AAILs,[38] as shown in Figure 3(d) in which the coordination number of CO_2-cation

22 and CO_2-anion were analyzed, respectively. It is found that the coordination number for CO_2 around [P_{4444}]

23 $^+$ cation is higher than that around anions. The same conclusions were drawn by Li *et al.* [38] in their simulation

24 study of the CO_2-metal based ILs. In addition, the coordination numbers ($N(r)$) of the CO_2-anion for all

25 CO_2-[P_{4444}][X] systems were calculated: N(CO_2-[Gly])=10.7, N(CO_2-[Im])=8.4, N(CO_2-[Pro])=6.3, N(CO_2-

26 [Suc])=6.0, N(CO_2-[Aps])=5.6 and N(CO_2-[Lys])=4.0. Therefore, for the chain-type amino acid anion, the

27 absorption capacity of the AAILs for CO_2 decreases as the increased chain length increases.
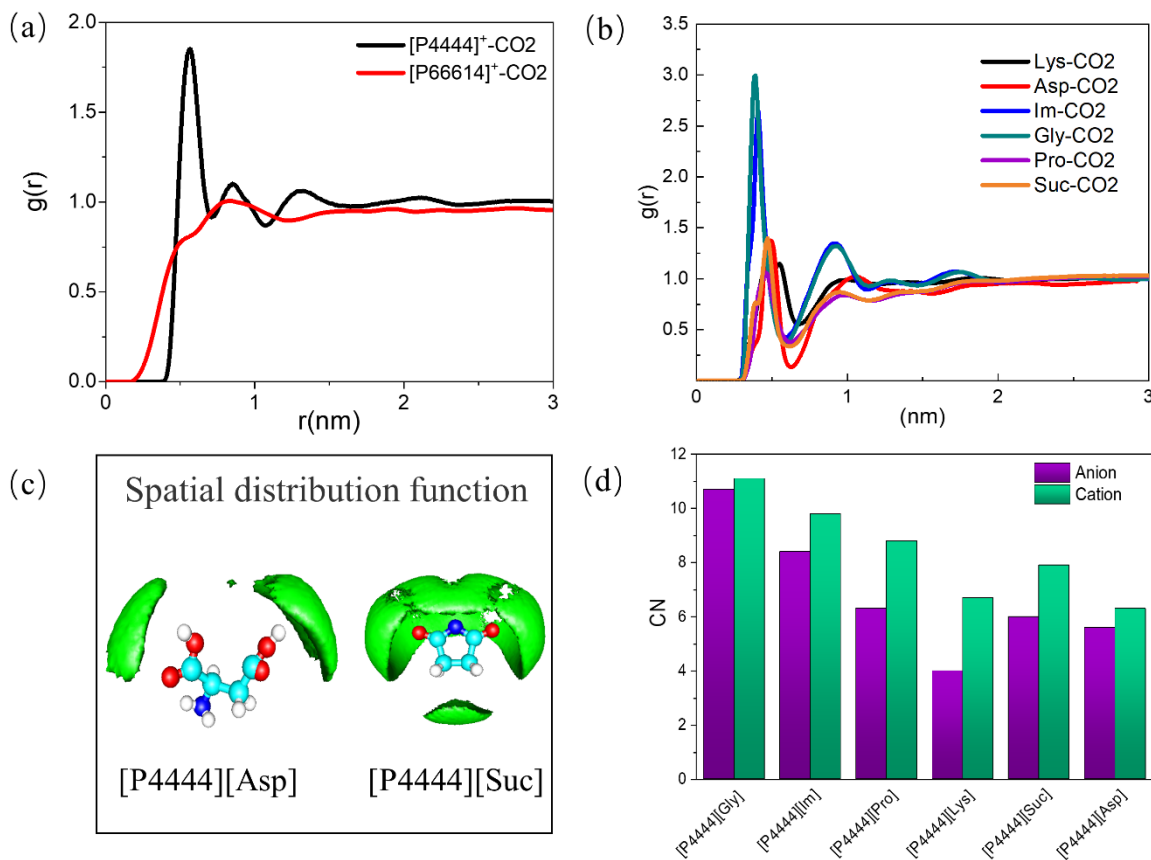
Figure 3. (a)-(b) Radial distribution function between CO_2 and the center of mass of cation and anion of [P_{4444}] [X] at 300 K. (c) The spatial distribution function for CO_2 molecules (green) around [Asp]$^{2-}$ and [Suc]$^-$ anion. (d)The coordination number between CO_2 and anion or cation in different AAIL systems at 300 K.

3.3.2 Stable Adsorption Sites

Herein, in order to demonstrate the stable absorption sites in the process of CO_2 absorption by AAILs, the site to site RDF and DFT method (mentioned in Section2.2) was used to analyze for anion-CO_2 in all systems. As Figure 4(b) shown, the site to site RDF of the carbon (C) atom from CO_2 molecular with the oxygen (O), nitrogen (N) and carbon (C) atoms from the anion of AAILs were investigated to shed light on the coordination mechanism of the CO_2 and AAILs. Take the CO_2-[P_{4444}] [Gly] system as an example, where the interactions of the C(CO_2)-O([Gly]), C(CO_2)-C([Gly]), C(CO_2)-P([Gly]), C(CO_2)-N([Gly]) were demonstrated. Obviously, the strengths of these interactions follow the order: C(CO_2)-O([Gly])> C(CO_2)-C([Gly]) > C(CO_2)-N([Gly]), implying that each CO_2 molecular preferentially coordinates with the O([Gly])

1   atoms in the carboxyl group, not the more electronegative N atom in amine group (-NH$_2$). This phenomenon

2   proves the importance of the carboxyl group in AAIL anion for CO_2 absorption.

3   Further, in order to clarify the role of the different type of anion with amino (-NH$_2$) and carboxyl (-

4   COOH) groups in AAILs in CO_2 absorption, the DFT calculations were performed on CO_2- anions to obtain

5   the optimized structure and the lowest interaction energy. As shown in Figure 4(a), for chain-type anion

6   (*eg.* [Gly]$^-$), the most stable site of CO_2 and anion is near the -COOH group, the distances between –COOH

7   group in [Gly]$^-$ and CO_2 were calculated to be 2.81 Å and 2.58 Å for O(-COOH) ···C (CO_2). This indicated

8   that the C atom in CO_2 molecule could equilibrate in the center of two O atoms in the carboxyl group,

9   meanwhile, the O=C=O bend angle is 169.36° and the lowest interaction energy of -11.95Kcal/mol. For

10   cyclic-type anion (such as [Pro]$^-$), the stable site is at the center of –COOH and –NH$_2$ group, the distance

11   between these two groups and CO_2 were calculated to be 2.56 Å for O···CO_2 and 2.83 Å for N···CO_2, the

12   O=C=O angles in [Pro]-CO_2 amount to 168.46°. This phenomenon proves that the amino acid anion for

13   improving the absorption of CO_2 by ILs through multiple site cooperation. In addition, the interaction

14   energy of CO_2-anion of [Asp]$^{2-}$, [Im]$^-$, [Gly]$^-$, [Lys]$^-$, [Suc]$^-$ and [Pro]$^-$ were -18.89Kcal/mol, -18.31Kcal/mol,

15   -11.95Kcal/mol, -10.35Kcal/mol, -9.48Kcal/mol and -9.27Kcal/mol, respectively. This indicated that the

16   chain-type structure of amino acid anion is more effective in absorbing CO_2 than cyclic-type anion. At the

17   same time, the Infrared Radiation (IR) spectrum of different CO_2-anion pairs were further calculated by

18   DFT calculations and shown in Figure 4(c). The obvious blue shift was exhibited of the vibrational mode

19   between C-O atom, where the frequency v(C-O) of [Asp]$^{2-}$, [Pro]$^-$, [Gly]$^-$, [Suc]$^-$ and [Lys]$^-$ are

20   546.7,571.4,572.8,618.8, and 624.9 cm^{-1}, respectively. This phenomenon due to the electron transfer from

21   the O atom to the CO_2 molecule. Meanwhile, the transferred electron could further enhance the C=O bond,

22   which agrees well with the vibration mode shown in Figure 4(c).

23
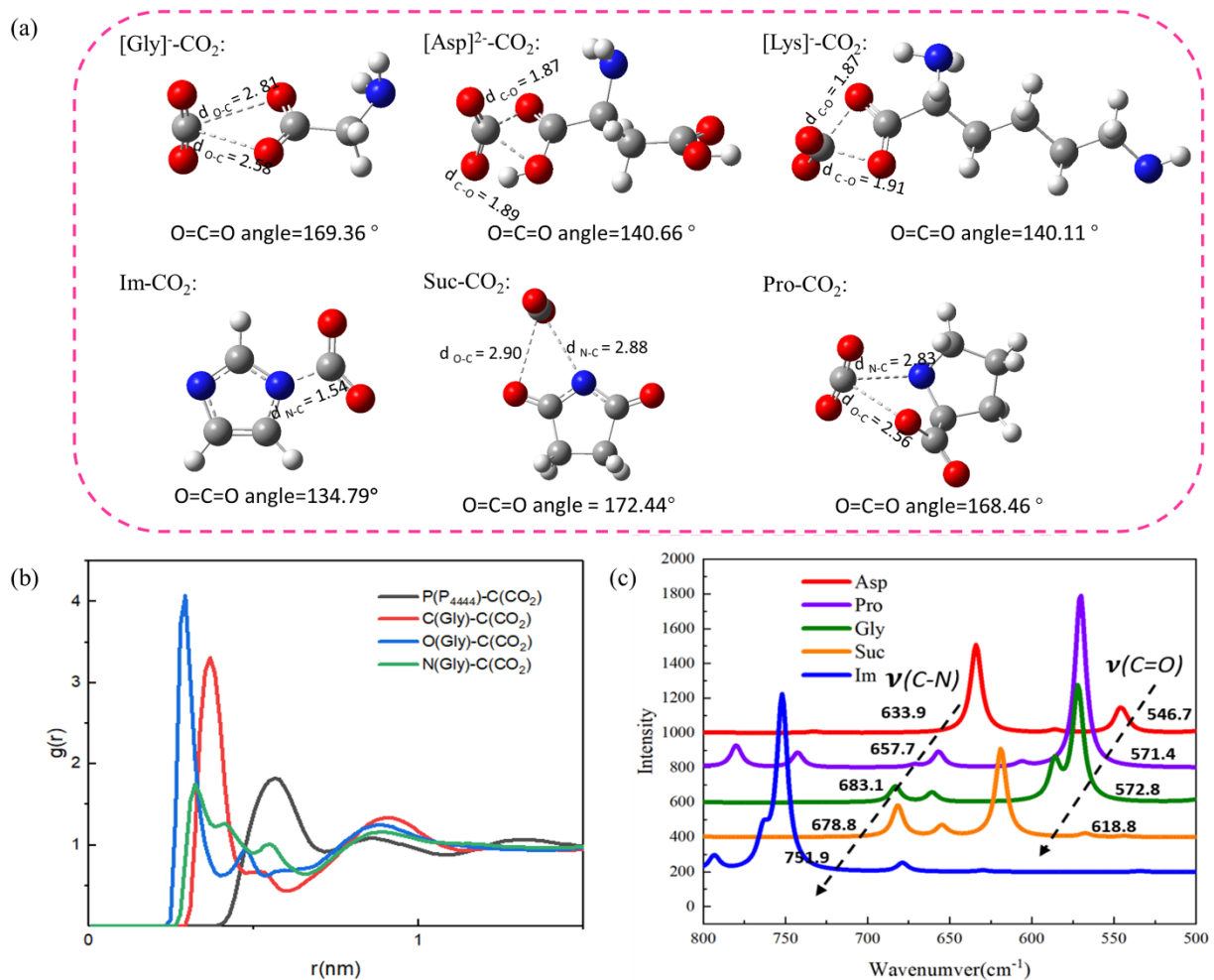
Figure 4. (a) The relaxed structure of CO_2-anion in different AAILs from the DFT calculations. (b) The site-site RDF between C/N/O atoms in -COOH, $-NH_2$ group of anion and C atom in CO_2 for [P$_{4444}$] [Gly]-CO_2 system at 300K. (c) The IR spectrum for different CO_2-anion pairs calculated from the DFT calculations.

3.3.3 Energic Interactions between CO_2 and Ionic Liquids.

To help understand the mechanism of cation and anion for CO_2 absorption in different AAILs, the van der Waals (vdW), electrostatic (elec) and total energy between the CO_2 molecular and AAILs were computed from 20NVT MD at varying temperatures (Table 3 and Table S2). It can be seen that the electrostatic energy is higher than the van der Waals energy for anion-CO_2 whereas an inverse trend is observed for cation-CO_2, which consistent with our previous research.[12] Meanwhile, the lower electrostatic

energy between cation and CO_2 is attributed to the more localized charge on the $[P_{4444}]^+$ cation. For CO_2-$[P_{4444}]$ [Gly] and CO_2-$[P_{4444}]$ [Im] the vdW interaction between CO_2 and the cation is about 10 times of the electrostatic energy. For the [Suc] anion that is like [Im] and is also symmetrical structure, the vdW energy of CO_2-$[P_{4444}]$ is significantly reduced, and the vdW energy is 5 times of the electrostatic energy. While, for the asymmetrical ring-type structure $[Pro]^-$, the vdW energy of CO_2-cation is reduced to 4 times the electrostatic energy. These results indicate that the interaction between CO_2 and the same cation also depends on the anion. The size and shape of the anion have a significant influence on the mechanism for CO_2 absorption in ILs. For CO_2-anion, the small size and asymmetry of [Gly] results in more "free" volume to accommodate CO_2, which leads to increased electrostatic interaction between CO_2 and anions. As the chain length increases, the electrostatic energy between anion and CO_2 gradually weakens. Furthermore, for the common cation ($[P_{4444}]^+$) the total energy of CO_2-AAILs follows the order: $[Gly]^- > [Im]^- > [Asp]^{2-} > [Lys]^- > [Suc]^- > [Pro]^-$. Interestingly, for the chain-type anion ($[Gly]^-$, $[Asp]^{2-}$ and $[Lys]^-$) the order were agree well with the coordination number (Section 3.3.1), indicating the lower interaction energy may lead to the more coordinate of CO_2 around the anion. In a word, the ILs with high CO_2 adsorption capacity need to possess both the strong van der Waals energy for the CO_2-cations and the electrostatic energy on the CO_2-anions. The same conclusion was also reported by Zhang *et al.*[39]

Table 3. Interaction Energy for all the AAILs-CO_2 systems

AAIL	Anion-CO_2(Kcal/mol)		Cation-CO_2(Kcal/mol)		Interatction Energy of AAIL-CO_2 (Kcal/mol)
	E_{ele}	E_{vdW}	E_{ele}	E_{vdW}	
$[P_{4444}][Gly]$	-3.68±0.10	-2.53±0.02	-1.01±0.05	-10.29±0.04	-17.51
$[P_{4444}][Im]$	-2.19±0.08	-2.75±0.03	-1.08±0.04	-10.38±0.06	-16.4
$[P_{4444}][Pro]$	-0.14±0.04	-1.71±0.03	-1.15±0.01	-4.59±0.08	-7.59
$[P_{4444}][Lys]$	--1.35±0.07	-3.11±0.06	-0.93±0.03	-6.73±0.11	-9.42
$[P_{4444}][Suc]$	-0.11±0.04	-1.94±0.04	-1.25±0.01	-5.05±0.09	-8.35
$[P_{4444}][Asp]$	-0.41±0.11	-1.15±0.03	-1.34±0.03	-6.65±0.12	-9.55

3.3.4 Effect on Microscopic Structure of Ionic Liquid by CO_2.

To further reveal the influence of the microstructure of AAILs on CO_2 absorption, especially the influence of anions with -COOH and -NH_2 groups on AAILs, three different RDFs for anion-anion, cation-cation and cation-anion were calculated. As shown in Figure 5 and Figure S3, the order of the position of the primary peak for RDF (anion-anion) is $[Im]^- < [Gly]^- < [Suc]^- < [Pro]^- < [Lys]^- < [Asp]^{2-}$, indicating the carboxyl group could enlarge the value of the distance of the first peak. At the same time, the position of the primary peak is positively correlated with the number of carboxyl groups, that is, the more carboxyl groups, the farther the position of the primary peak is. For RDF (cation-cation), most of the first peak positions are around 0.82nm, however for $[Lys]^-$ anion, the position of the first peak in the g(r) plot of the cation-cation shifts backward from 0.81nm to 1.1nm (Figure S3). This result indicates that the longer-chain amino acid anion has a greater influence on the cation microstructure. Interestingly, the order of position of the first peak for cation-anion is consistent with that of the anion-anion, indicates that the structure of anions in AAILs can be used as an effective variable to adjust the microstructure of ILs. Therefore, amino acid anions, especially the anions of two carboxyl groups, have the greatest impact on the structure of AAILs, which can effectively promote the absorption of carbon dioxide molecules. Besides, in order to quantitatibe describe the changes in the microstructure of AAILs caused by CO_2, the coordination number also calculated for anion-anion, cation-cation and cation-anion pairs and shown in Figure 5(b). It can be seen that the order of the coordination number for cation around anions is $[Lys]^- < [Pro]^- < [Suc]^- < [Asp]^{2-} < [Im]^- < [Gly]^-$, which is consistent with the coordination number for cation around cation. The observations further demonstrated the $[Gly]^-$ anion has the best absorption capacity, meanwhile, due to the larger size of $[Lys]^-$ and $[Pro]^-$, the coordination number is lower. Therefore, we have reason to believe that the size of anion in AAILs is a key factor affecting CO2 absorption, and this phenomenon is crucial to the design of AAILs on molecular level.
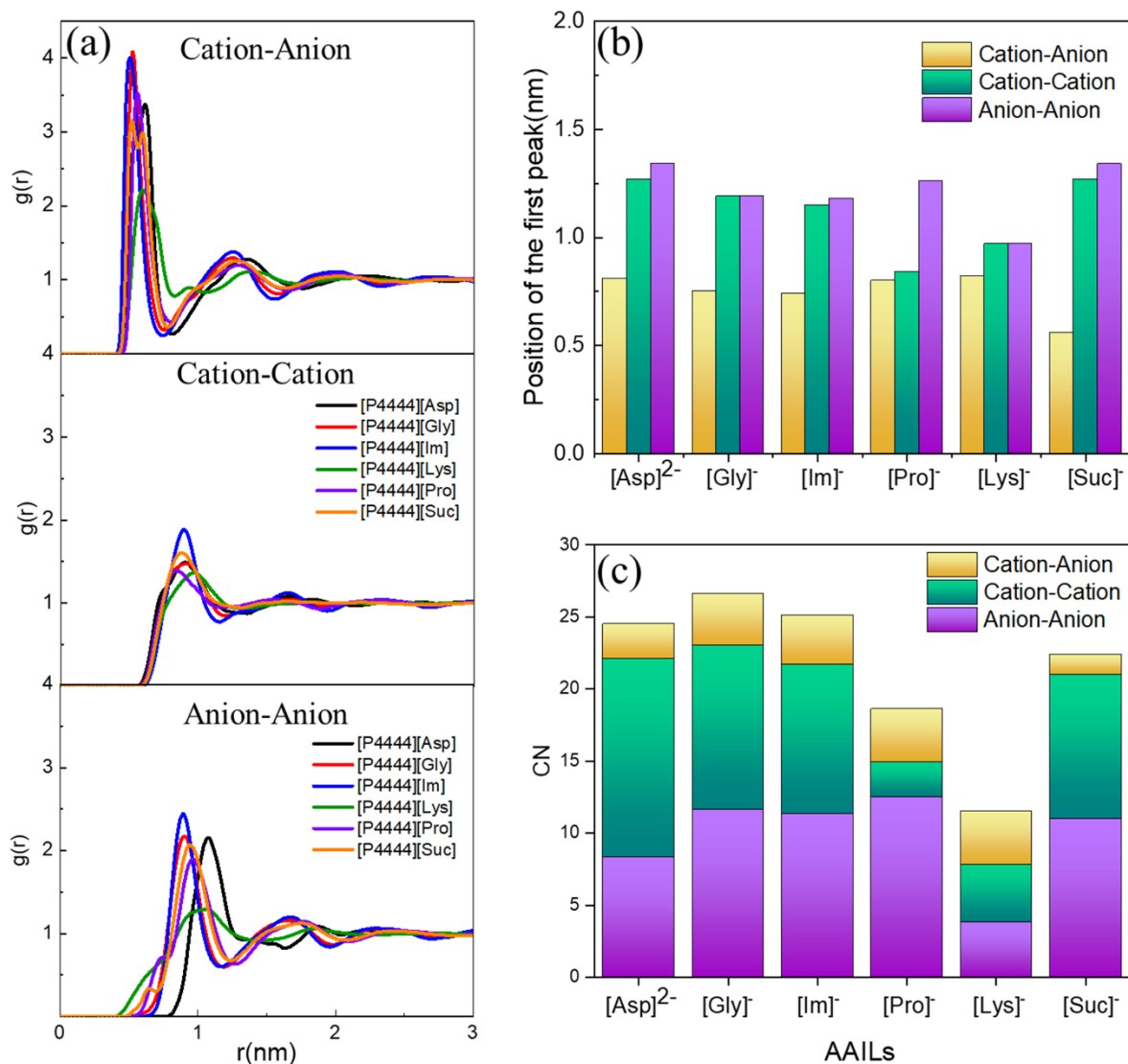
Figure 5. (a) The center of mass RDF for anion-anion cation-cation and cation-anion pair. (b) The position of the first peak for three types of RDFs; (c) The coordination number of anion-anion, cation-cation, and cation-anion pairs in [P_{4444}] [X] ([X]=[Asp]$^{2-}$, [Gly]$^-$, [Im]$^-$, [Lys]$^-$, [Pro]$^-$, and [Suc]$^-$) at 300 K.

4. Conclusions

Amino acid ionic liquids used as absorbents in gas absorption could improve the efficiency and greenness of the absorption process, thereby increasing the ability to resist climate warming. Fundamental molecular insights are useful for understanding the advantages of AAILs. In this work, atomic MD

simulations and first-principles calculations are used to study the capabilities and effects of six different ionic liquids with amino and carboxyl groups in absorbing CO_2.

We firstly calculated the density and dynamics properties of all the CO_2-AAILs systems. Simulation results revealed that the larger size of cation have lower density and larger self-diffusion coefficient. At the same time, the density and kinetic characteristics of the system increase with the increase of the number of anionic carboxyl groups. For anions of similar size, chain-type anions perform better in dynamic characteristics than cyclic-type anions. Later, we evaluated the radial distribution function (g(r), spatial distribution function (sdf), coordination number, intermolecular interaction energy (vdW and electrostatic energy)) to clarify the effect of different amino acid ionic liquids on the absorption of CO_2 Influence and internal mechanism. At the same time, DFT analysis and site-to-site RDF calculations revealed the stable absorption sites of AAILs in the absorption of CO_2. The result indicated that due to the steric hindrance caused by the phosphorus atoms with a large number of positive charges and with longer alkyl chains on the cations, the interaction between the CO_2 molecules and the cations in AAILs is weak. Meanwhile, we realized that the absorption of CO_2 in AAILs is an anion-driven process. The coordination number and interaction energy jointly suggest that the absorbing capacity of AAILs increasing in the order $[Asp]^{2-}$, $[Suc]^-$, $[Lys]^-$, $[Pro]^-$, $[Im]^-$, $[Gly]^-$. At the same time, it is more effective to absorb CO_2 through chain AAIL instead of cyclic AAIL. And the alkyl chain in the chain anion will affect the absorption between the anion and CO_2, that is, the longer the alkyl chain will hinder the free movement of CO_2 molecules in the CO_2-AAILs system, and affect the absorption efficiency. The calculation result of DFT proves that absorption of CO_2 is a multi-site cooperative way by AAILs. For chain anions, the most stable sites for CO_2 and anions are located at the center of the two O atoms in the -COOH group, and for cyclic anions, the stable site is located at the center of the -COOH and -NH_2 groups. Therefore, in the molecular design strategy of AAILs, short chain-type anions or anions with a large number of -COOH groups should be prioritized to enhance the performance of IL in the CO_2 absorption process.

Conflicts of interest

The authors declare no conflicts of interest.

Acknowledgment

References

1 I. I. Alkhatib, C. Garlisi, M. Pagliaro, K. Al-Ali and G. Palmisano, *Catal. Today*, 2020, **340**, 209-224.

2 N. Zhang, Z. Pan, Z. Zhang, W. Zhang, L. Zhang, F. M. Baena-Moreno and E. Lichtfouse, *Environ. Chem. Lett.*, 2020, **18**, 79-96.

3 Z. Zhang, J. Muschiol, Y. Huang, S. B. Sigurdardóttir, N. Von Solms, A. E. Daugaard, J. Wei, J. Luo, B. H. Xu, S. Zhang and M. Pinelo, *Green Chem.*, 2018, **20**, 4339-4348.

4 H. Yan, L. Zhao, Y. Bai, F. Li, H. Dong, H. Wang, X. Zhang and S. Zeng, *ACS Sustain. Chem. Eng.*, 2020, **6**, 2523-2530.

5 S. Zeng, L. Liu, D. Shang, J. Feng, H. Dong, Q. Xu, X. Zhang and S. Zhang, *Green Chem.*, 2018, **20**, 2075-2083.

6 S. Yuan, X. Li, J. Zhu, G. Zhang, P. Van Puyvelde and B. Van Der Bruggen, *Chem. Soc. Rev.*, 2019, **48**, 2665-2681.

7 H. Sanaeepur, A. Ebadi Amooghin, S. Bandehali, A. Moghadassi, T. Matsuura and B. Van der Bruggen, *Prog. Polym. Sci.*, 2019, **91**, 80-125.

8 F. Huo and Z. Liu, *Mol. Simulat.*, 2015, **41**, 271-280.

9 S. Zhang, Y. Wang, H. He, F. Huo, Y. Lu, X. Zhang and K. Dong, *Green Energy Environ.*, 2017, **2**, 329-330.

10 M. Hasib-ur-Rahman, M. Siaj and F. Larachi, *Chem. Eng. Process.*, 2010, **49**, 313-322.

11 X. Zhang, X. Zhang, H. Dong, Z. Zhao, S. Zhang and Y. Huang, *Energy Environ. Sci.*, 2012, **5**, 6668-6681.

12 X. Zhang, F. Huo, Z. Liu, W. Wang, W. Shi and E. J. Maginn, *J. Phys. Chem. B*, 2009, **113**, 7591-7598.

13 C. Wang, S. M. Mahurin, H. Luo, G. A. Baker, H. Li and S. Dai, *Green Chem.*, 2010, **12**, 870-874.

14 C. S. Lee, N. U. Kim, J. T. Park and J. H. Kim, *Sep. Purif. Technol.*, 2020, **242**, 116780.

15 A. R. Shaikh, M. Ashraf, T. AlMayef, M. Chawla, A. Poater and L. Cavallo, *Chem. Phys. Lett.*, 2020, **745**, 137239.

16 V. Sang Sefidi and P. Luis, *Ind. Eng. Chem. Res.*, 2019, **58**, 20181-20194.

17 S. Chong, T. Wang, H. Zhong, L. Xu, H. Xu, Z. Lv and M. Ji, *Green Energy Environ.*, 2020, **5**,

154-165.

18   K. Fukumoto, M. Yoshizawa and H. Ohno, *J. Am. Chem. Soc.*, 2005, **127**, 2398-2399.

19   C. Wang, X. Luo, H. Luo, D. E. Jiang, H. Li and S. Dai, *Angew. Chem. Int. Edit.*, 2011, **50**, 4918-4922.

20   Y. Huang, G. Cui, Y. Zhao, H. Wang, Z. Li, S. Dai and J. Wang, *Angew. Chem. Int. Edit.*, 2017, **56**, 13293-13297.

21   F. Moghadam, E. Kamio and H. Matsuyama, *J. Membrane Sci.*, 2017, **525**, 290-297.

22   B. Seyedhosseini, M. Izadyar and M. R. Housaindokht, *J. Phys. Chem. A*, 2017, **121**, 4352-4362.

23   S. Kang, Y. G. Chung, J. H. Kang and H. Song, *J. Mol. Liq.*,2020, **297**, 111825.

24   R. Sen, A. Goeppert, S. Kar and G. K. S. Prakash, *J. Am. Chem. Soc.*, 2020, **142**, 4544-4549.

25   Y. Guo, C. Li, S. Lu and C. Zhao, *Chem. Eng. J.*, 2016, **301**, 325-333.

26   E. J. Maginn, *J. Phys. Condens. Matter.Phys*, 2009, **21**, 373101.

27   M. Salanne, *Phys. Chem. Chem. Phys.*, 2015, **17**, 14270–14279.

28   L. Martínez, R. Andrade, E. G. Birgin and J. M. Martínez, *Softw. News Updat.*, 2009, **30**, 2157–2164.

29   D. Van Der Spoel, E. Lindahl, B. Hess, G. Groenhof, A. E. Mark and H. J. C. Berendsen, *J. Comput. Chem.*, 2005, **26**, 1701–1718.

30   M. J. Frisch, G.; Trucks, W.; Schlegel, H. B. .; Scuseria, G. E. .; Robb, M. A. .; Cheeseman, J. R.; Scalmani, G.; Barone, V. .; Mennucci, B. .; Petersson, G. A.; et al. *Gaussian 09, Revision E. 01; Gaussian*; 2009.

31   K. R. Seddon, A. Stark and M.-J. Torres, 2000, *Pure Appl. Chem.*, **72**, 2275-2287 .

32   B. F. Goodrich, J. C. De La Fuente, B. E. Gurkan, D. J. Zadigian, E. A. Price, Y. Huang and J. F. Brennecke, *Ind. Eng. Chem. Res.*, 2011, **50**, 111-118.

33   J. Zhang, S. Zhang, K. Dong, Y. Zhang, Y. Shen and X. Lv, *Chem. - Eur. J.*, 2006, **12**, 4021-4026.

34   M. H. Kowsari, S. Alavi, M. Ashrafizaadeh, and B. Najafi, *J. Chem. Phys.*, 2008, **129**, 224508.

35   W. Ren, B. Sensenich and A. M. Scurto, *J. Chem. Thermodyn.*, 2010, **42**, 305-311.

36   P. Prakash and A. Venkatnathan, *RSC Adv.*, 2016, **6**, 55438.

37   S. G. Kazarian, N. Sakellarios and C. M. Gordon, *Chem. Commun.*, 2002, **12**, 1314-1315.

38   B. Li, C. Wang, Y. Zhang and Y. Wang, *Green Energy Environ.*, DOI:10.1016/j.gee.2020.04.009.

39   X. Zhang, K. Jiang, Z. Liu, X. Yao, X. Liu, S. Zeng, K. Dong and S. Zhang, *Ind. Eng. Chem. Res.*, 2018, **58**, 1443–1453.